

Zero-TPrune: Zero-Shot Token Pruning through Leveraging of the Attention Graph in Pre-Trained Transformers

Hongjie Wang, Bhishma Dedhia, Niraj K. Jha
 Princeton University
 Princeton, NJ 08540, USA
 {hongjiewang, bdedhia, jha}@princeton.edu

Abstract

Deployment of Transformer models on edge devices is becoming increasingly challenging due to the exponentially growing inference cost that scales quadratically with the number of tokens in the input sequence. Token pruning is an emerging solution to address this challenge due to its ease of deployment on various Transformer backbones. However, most token pruning methods require computationally expensive fine-tuning, which is undesirable in many edge deployment cases. In this work, we propose Zero-TPrune, the first zero-shot method that considers both the importance and similarity of tokens in performing token pruning. It leverages the attention graph of pre-trained Transformer models to produce an importance distribution for tokens via our proposed Weighted Page Rank (WPR) algorithm. This distribution further guides token partitioning for efficient similarity-based pruning. Due to the elimination of the fine-tuning overhead, Zero-TPrune can prune large models at negligible computational cost, switch between different pruning configurations at no computational cost, and perform hyperparameter tuning efficiently. We evaluate the performance of Zero-TPrune on vision tasks by applying it to various vision Transformer backbones and testing them on ImageNet. Without any fine-tuning, Zero-TPrune reduces the FLOPs cost of DeiT-S by 34.7% and improves its throughput by 45.3% with only 0.4% accuracy loss. Compared with state-of-the-art pruning methods that require fine-tuning, Zero-TPrune not only eliminates the need for fine-tuning after pruning but also does so with only 0.1% accuracy loss. Compared with state-of-the-art fine-tuning-free pruning methods, Zero-TPrune reduces accuracy loss by up to 49% with similar FLOPs budgets. Project webpage: <https://jha-lab.github.io/zerotprune>.

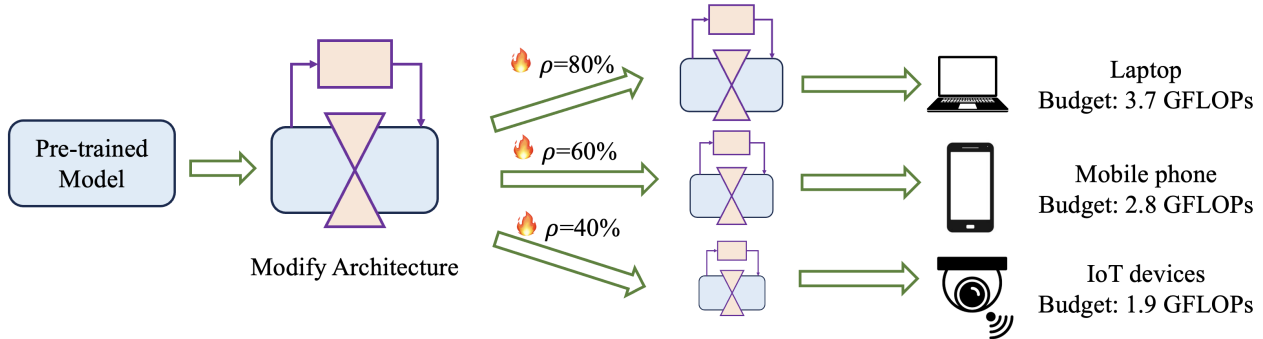
1. Introduction

The Transformer [37] architecture has emerged as a *de facto* workhorse of contemporary machine learning paradigms,

showing impressive generalization across a swath of tasks including Computer Vision (CV) [34], natural language processing (NLP) [10], robotics [31], and games [26]. At the heart of the architecture lies the multi-headed self-attention that dynamically aggregates parallel-processed tokens, yielding a highly effective general-purpose computing framework. The implications are particularly apparent in the case of CV where the Transformer’s ability to assimilate rich abstractions from large-scale data facilitates strong transfer to downstream tasks, outperforming state-of-the-art Convolutional Neural Networks (CNNs) [12].

Studies on empirical scaling laws for Vision Transformers (ViTs) [41] point to the possibility of improvement in model performance with model capacity; recent models have indeed been scaled to billions of parameters. While model scaling brings with it the promise of remarkable generalization, it poses serious obstacles to deploying such architectures on compute-constrained devices like the edge and executing real-time inference workloads under limited energy and memory. *How does one reduce the computational complexity of the forward pass while still maintaining the richness of learned representations?* To this end, *Token Pruning* opens up a promising avenue. Drawing a simple analogy to the human vision system, when trying to identify an exotic bird perched on the window on an idyllic afternoon, we tend to prune away inconsequential visual details like the cup of piping hot tea lying nearby, the ambling pedestrians on the walkway or the sunlit foliage in the background. The attention heads induce quadratic computational complexity with respect to the input sequence length. Thus, pruning unimportant tokens can result in significant speedups, especially in the case of longer sequences. Since token pruning only prunes the information that passes through the sequential layers of the Transformer and does not necessitate architectural modifications to the backbone, it can be widely deployed on most Transformer backbones and any computational hardware can fully exploit the resultant sparsity. However, most existing token pruning methods rely on token scoring mod-

Most existing methods: expensive re-training 🔥 is required for each configuration



Our method: pruning deployment is training-free and can switch between different configurations at no computational cost ❄️

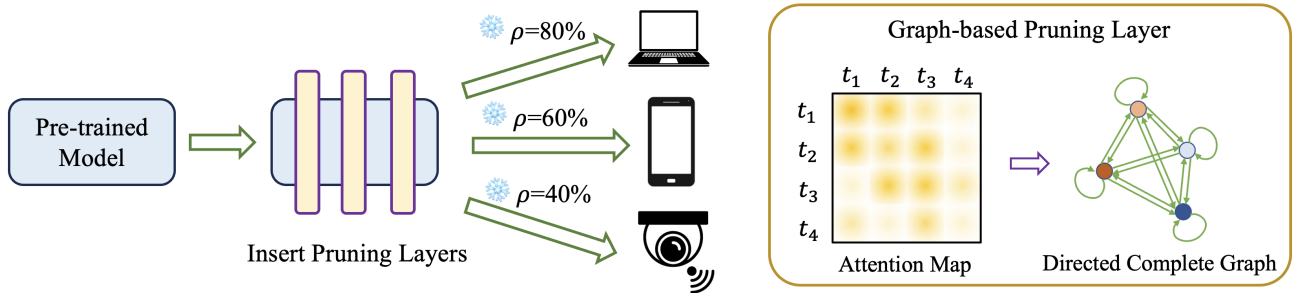


Figure 1. Comparing existing efficiency enhancement methods and Zero-TPruning. ρ represents the retention ratio measured by FLOPs cost. Most existing methods require re-training of the model after deploying it; each different pruning configuration requires separate re-training of the model, which is extremely expensive. On the contrary, Zero-TPruning is training-free and can switch between different pruning configurations at no computational cost. This benefits from our graph-based algorithm exploiting correlations between image tokens.

ules that must be trained together with the backbone, requiring computationally-expensive re-training or fine-tuning for deployment. This is impractical for edge applications and users, given the scarcity of computing resources. For example, the state-of-the-art token pruning method DynamicViT [30] requires 150 hours of fine-tuning on an NVIDIA A100 GPU to prune the DeiT-S [36] model. Moreover, the memory and computational resources available may differ widely across edge devices; they may also have wide variations in throughput requirements. Fine-tuning-required pruning methods need to train the model repeatedly under different pruning configurations imposed by hardware constraints, as shown in Fig. 1, making the pruning process even more expensive. In addition, these methods are impractical for pruning very large models due to the high computation overhead of training after pruning. For instance, thousands of A100 GPU hours are needed to apply DynamicViT [30] to the DeiT-B and DeiT-L models [36].

In this work, we propose a *training-free* zero-shot token pruning method called Zero-TPruning. *How does one prune tokens without fine-tuning?* The soft attention between tokens induces a directed graph with tokens as nodes and attention as edges. Edge strengths indicate attention values. We posit and later show through a rigorous and comprehensive set of experiments that the attention graph is a rich information source for inferring important tokens and, con-

versely, tokens that can readily be pruned. *How does one identify important tokens from the attention graph?* The weights of the directed edges on the attention graph can be interpreted as information routing volume between nodes. Utilizing the underlying assumption that other important tokens attend to important tokens, we iteratively assign relative importance to tokens. Such ranking methods [4] have been ubiquitously used by search engines to organize web pages on the Internet. *Can one further exploit redundancy among tokens?* Our experiments show that tokens often learn similar abstractions and, therefore, copies of the same feature can be pruned without loss of information. We augment importance ranking with similarity-driven pruning to account for similar tokens. Although Zero-TPruning can potentially be applied to any Transformer-based tasks, we focus on vision tasks to evaluate its performance in this article.

The main contributions of this work can be summarized as follows. (1) We present Zero-TPruning, a zero-shot token pruning method that efficiently leverages the feature identification capability (considers the attention matrix as an adjacency matrix of a directed graph) of pre-trained Transformers. It exploits both the importance and similarity of tokens to perform pruning. (2) We use a graph signal to represent the importance score distribution on tokens and propose the Weighted Page Rank (WPR) algorithm to infer unimportant tokens during iterative importance assignment.

This iterative scheme reduces noise from unimportant tokens during assignment. (3) Instructed by the importance distribution, we partition tokens into two groups and perform similarity-based pruning. Input-dependent partitioning controls the importance distribution of tokens pruned by the similarity metric. (4) We apply Zero-TPPrune and baseline methods to various Transformer backbones and evaluate their performance on ImageNet [9]. The used backbones include DeiT [36], LV-ViT [18], AugReg [33], etc. Compared with state-of-the-art fine-tuning-required Transformer pruning methods, Zero-TPPrune eliminates the need for fine-tuning after pruning DeiT-S with only around 0.1% accuracy reduction while achieving the same FLOPs saving. Moreover, Zero-TPPrune outperforms state-of-the-art fine-tuning-free methods in terms of both accuracy and throughput. Zero-TPPrune reduces accuracy loss by 33% on DeiT-S when compared with state-of-the-art fine-tuning-free methods. In terms of throughput, Zero-TPPrune provides 45.3% off-the-shelf speed-up at a cost of only 0.4% in accuracy.

2. Related Works

In the first few years after the Transformer model was proposed in 2017, it was mainly employed in the NLP field [10]. ViT [12] was the first work to directly apply an *encoder-only* Transformer architecture to non-overlapping image patches in an image classification task without employing any convolution operations. Relative to state-of-the-art CNNs, ViT was able to achieve better performance through large-scale pre-training. DeiT [36] was another convolution-free Transformer that was trained only on ImageNet [9] and achieved better performance than ViT by relying on several training techniques. Both ViT and its follow-up architectures split the input image into multiple non-overlapping image patches and transform them into tokens for further processing. This provides a new dimension to sparsity exploitation that is quite different from sparsity-enhancing techniques employed in CNNs.

Most of the previous token pruning works focus on NLP tasks, including PoWER-BERT [15], Length-Adaptive Transformer [19], SpAtten [39], TR-BERT [42], and Learned Token Pruning [20]. For CV tasks, a typical token pruning work is DynamicViT [30]. It inserts prediction modules between transformer blocks to predict and drop less informative tokens. The prediction modules are neural networks that can be jointly trained with the vision Transformer backbone. Instead of using a deterministic strategy to prune tokens, A-ViT [43] introduces a stochastic pruning process. It uses adaptive halting modules to compute the halting probability per token. A token is pruned (i.e., discarded) upon reaching the halting condition. As a result, the number of tokens is gradually reduced, leading to faster inference. Other recent works on token pruning for ViT include SPViT [21], TPS [40], Adaptive Sparse ViT [24],

DToP [35], and HeatViT [11]. Although the pruning methods mentioned above require few or even no extra parameters for pruning, they require computationally-expensive fine-tuning after pruning. On the contrary, our proposed Zero-TPPrune can eliminate the training process after pruning with only 0.1% accuracy reduction.

There are a few previous works that have explored pruning tokens without requiring fine-tuning. ATS [14] uses an inverse transform to accomplish adaptive token sampling based on the importance score distribution. When the importance scores are concentrated on several tokens, the number of sampled tokens automatically reduces. However, ATS only uses the attention probability of the classification (CLS) token in the attention matrix and ignores the effect of similarity between tokens. ToMe [3], on the other hand, focuses on merging tokens instead of pruning them, thereby reducing the inference overhead of pre-trained Transformers without fine-tuning. Tokens are progressively merged based on their similarity as the layers become deeper. However, ToMe solely relies on embedding vectors from pre-trained models and its matching process lacks appropriate guidance (more details in Section 3.3). In contrast, Zero-TPPrune effectively utilizes both the complete attention matrix and embedding vectors from pre-trained Transformers, while simultaneously considering the importance and similarity of tokens.

3. Methodology

In this section, we first provide an overview of Zero-TPPrune in Section 3.1, then describe its components, **I-stage** (Section 3.2) and **S-stage** (Section 3.3). Note that Zero-TPPrune is potentially differentiable, which enables the pruned model to be further fine-tuned for better performance. This optional training-after-pruning paradigm is described in Supplementary Material Section C.

3.1. Overview: Zero-TPPrune

The overall Zero-TPPrune framework is shown in Fig. 2. Each pruning layer is composed of multiple stages and can be inserted anywhere between Transformer blocks. The **I-stage** and **S-stage** enable Zero-TPPrune to take both importance and similarity into consideration. The objective of the **I-stage** is to obtain an importance score distribution on tokens and retain the top- k important tokens. To achieve this objective, we propose the WPR algorithm and use the attention matrix from the pre-trained Transformer block. In the **S-stage**, we measure the similarity between tokens based on their embedding vectors and retain only one token in the top- r similar pairs. To reduce computational overheads from all pair-wise combinations, we partition tokens into bipartite groups. Tokens in the same group are never paired to measure similarity. To have improved control over the

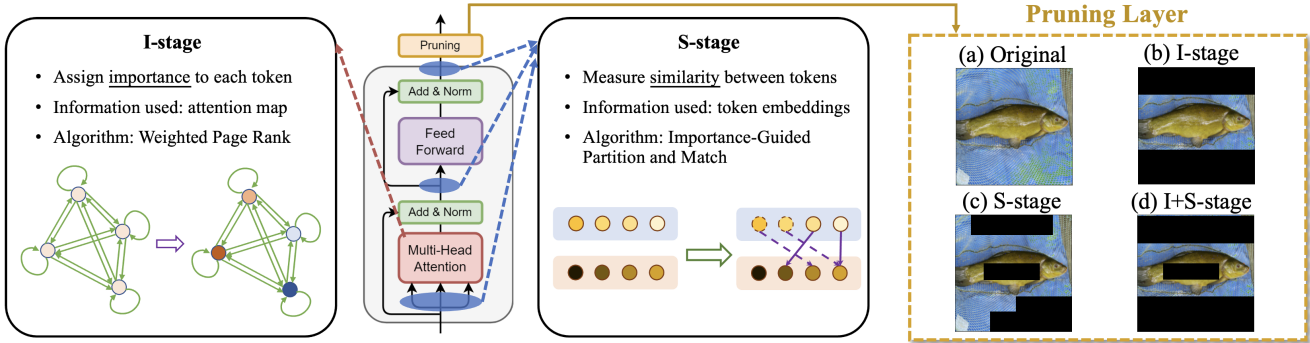


Figure 2. The overall Zero-TPrune framework. Pruning layers can be inserted between Transformer blocks to reduce the number of tokens. Pruning layers comprise **I-stage** and **S-stage**: **I-stage** aims at pruning unimportant tokens of an image, such as background tokens (see (b)); **S-stage** aims at pruning tokens that are too similar to others, such as repetitive texture tokens (see (c)). A combination of the stages then maximally exploits token redundancy (see (d)).

importance distribution of pruned tokens, we guide the partitioning by their importance rank.

A straightforward way to combine the two stages is to consecutively connect the **I-stage** and **S-stage**: some tokens are pruned based on the obtained importance score distribution in the **I-stage**; this distribution is then used to guide the partition in the **S-stage** and some other tokens are pruned based on similarity. However, we empirically observed that such a trivial combination may cause the semantically unimportant tokens to eventually crowd out semantically significant tokens in the **I-stage**. For example, sometimes background tokens received high importance scores compared to the main object tokens. Details of this phenomenon can be found in Supplementary Material Section A.1. We resolve this issue by interchanging the **I-stage** and **S-stage**. This method enables the early elimination of similar tokens in the **S-stage**, consequently reducing the adverse impact of similarity in the **I-stage** to a significant extent. We present a comparison of the two patterns in Supplementary Material Section A.2. To facilitate partitioning in the **S-stage**, we introduce a pre-ranking **I'-stage** to assign importance scores to tokens with a *single* round of voting. Notably, no token is pruned in the **I'-stage**. Consequently, the pruning layer comprises sequential application of **I'-stage**, **S-stage**, and **I-stage**.

3.2. I-stage: Importance-based Pruning

To retain the top- k important tokens, we introduce a ranking metric called *importance score*. In order to obtain the importance score, we treat attention matrix $\mathbf{A}^{(h,l)}$ as the adjacency matrix of a complete, directed graph, called the *attention graph*, as shown in Fig. 3(a). Ranking nodes in the graph is challenging because of several reasons. (i) The attention graph is dense, usually including hundreds of nodes and many more edges when the input is an image. (ii) We have a strict budget for the computational overhead incurred by the per-image algorithm during inference.

Inspired by the Page Rank [4] algorithm, we propose a

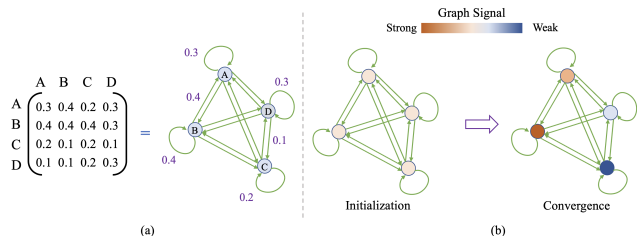


Figure 3. Overview of the I-stage: (a) from a 4×4 attention matrix to an attention graph and (b) graph signal transformation from initialization to convergence.

WPR algorithm to derive the importance scores. Page Rank was used in Google Search for ranking web pages. In the original Page Rank algorithm, links between web pages are unweighted. In order to apply it to the weighted and directed attention graph, we consider the signal of each node in this graph as the importance of each token. We initialize the graph signal uniformly and use the adjacency matrix as a Graph Shifting Operator (GSO). When the GSO is applied to the graph signal, each node votes for which node is more important through the weight assigned to output edges, i.e., the attention that a token pays to other tokens. If the node itself is more important, the voting of this node is more important. This is shown in Algorithm 1. The transition from initialization to convergence is shown in Fig. 3(b).

We obtain the expression for the importance score of each node (i.e., token) in the l -th layer, h -th head as follows:

$$s^{(h,l)}(x_i) = \frac{1}{N} \sum_{j=1}^N \mathbf{A}^{(h,l)}(x_i, x_j) \cdot s^{(h,l)}(x_j) \quad (1)$$

where $s^{(h,l)}(x_j)$ is the importance score of node x_i in the h -th head of the l -th layer, and N is the number of tokens in the l -th layer. $s^{(h,l)}(x_i)$ is derived from the weighted sum of the received attention. WPR thus recursively assigns high importance to semantically significant tokens and reduces noise from unimportant semantically weak tokens. We retain the top- k important tokens (k is determined by the retention rates and the total number of tokens).

Algorithm 1 Graph-based Weighted Page Rank (WPR) algorithm

Require: $N > 0$ is the number of nodes in the graph; $A \in \mathbb{R}^{N \times N}$ is the adjacency matrix of this graph; $s \in \mathbb{R}^N$ represents the graph signal

Ensure: $s \in \mathbb{R}^N$ represents the importance score of nodes in the graph

$s^0 \leftarrow \frac{1}{N} \times e_N$ \triangleright Initialize the graph signal uniformly
 $t \leftarrow 0$

while ($|s^t - s^{t-1}| > \epsilon$) **or** ($t = 0$) **do** \triangleright Continue iterating if not converged

$t \leftarrow t + 1$

$s^t \leftarrow A^T \times s^{t-1}$ \triangleright Use the adjacency matrix as a graph shift operator

end while

$s \leftarrow s^t$

Simply averaging the importance scores across different heads is not the optimal choice. Different heads in an encoder layer usually pay attention to different parts of the input image (a visual example is given in Supplementary Material Section E.1). Thus, there are some tokens that are very important in one or two heads, but not in others. On the other hand, some tokens have low-to-medium importance in all heads. The former tokens are usually more informative than the latter tokens. However, if there are multiple heads and the importance score is directly averaged across all heads, the latter tokens may get the same or even higher score than the former tokens, leading to incorrect token ranking and pruning. In order to address this problem, we aggregate the importance scores across heads via a root-mean of sum of squares. We call this the Emphasizing Informative Region (EIR) aggregation. We observe that EIR effectively distinguishes informative areas from non-informative ones. A concrete example that compares EIR with other methods (such as *argmax* and average) is given in Supplementary Material Section E.1.

Besides the issue mentioned above, sometimes the importance scores given by the WPR algorithm may converge to an undesired distribution in some heads: (1) tokens at the edge of the input image may get very high importance scores; (2) the importance score distribution may become nearly uniform. We provide visual examples of these cases in Supplementary Material Section E.2. Both heads in these cases do not provide helpful information and are even misleading. To mitigate the negative impact of these heads, we introduce the Variance-based Head Filter (VHF). We compute the variance of the distribution in each head and set both a minimum and a maximum threshold for the variance. Heads with a distribution variance exceeding the maximum threshold or falling below the minimum threshold are excluded from the computation. Then the final importance

score equation becomes:

$$s^{(l)}(x_i) = \sqrt{\frac{\sum_{h=1}^{N_h} s^{(h,l)}(x_i)^2 \cdot \eta(v_{\min} \leq Var_h \leq v_{\max})}{\sum_{h=1}^{N_h} \eta(v_{\min} \leq Var_h \leq v_{\max})}} \quad (2)$$

where $\eta(v_{\min} \leq Var_h \leq v_{\max})$ equals 1 if $v_{\min} \leq Var_h \leq v_{\max}$, otherwise it equals 0; v_{\min} and v_{\max} represent the minimum and maximum threshold, respectively; Var_h is the importance score variance of tokens in the h -th head; N_h is the number of heads in the l -th layer. The complexity of **I-stage**, including WPR, EIR, and VHF, is $O(N^2)$, where N is the number of tokens.

3.3. S-stage: Similarity-based Pruning

As discussed previously, it is valuable to measure similarity even between important tokens and perform further pruning. Previous work [3] uses image-agnostic token partitioning to measure pair-wise similarity. Instead, we propose a per-image importance-driven partition for similarity pruning, as shown in Fig. 4.

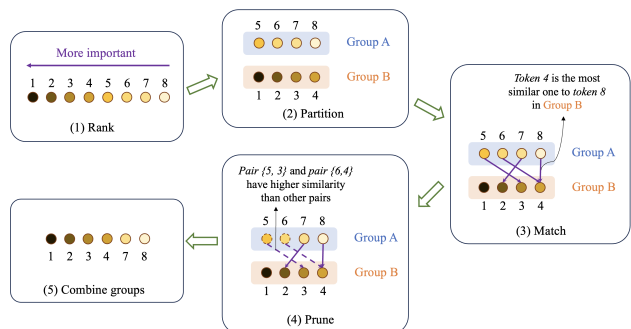


Figure 4. The importance-based pruning process in the S-stage. As an example, sequential partitioning (pruning unimportant part) is used in this figure.

Fig. 4 (1&2): Based on the importance score of tokens, we sequentially partition them into groups of roughly equal size, A and B , and prune the less important group. We explore other importance-guided partitioning schemes, including alternative partitioning and random partitioning, and provide ablation results in Supplementary Material Section G.3. **Fig. 4 (3):** We then identify the most similar token in Group B for each token in Group A and record the corresponding similarity of each pair. To accomplish this, we represent each token by a feature vector, which can be derived from several available choices, such as corresponding vectors in the Key, Query, or Value matrix. Our ablation experiments indicate that using vectors from the Key matrix is the optimal choice. We compute similarity on these vectors using a designated metric, such as cosine similarity, Manhattan distance, or Euclidean distance. Following the results of our ablation experiments, we employ cosine similarity. We provide a detailed account of our ablation experiment outcomes in Supplementary Material Section G.3.

Fig. 4 (4&5): In the next step, we select top- r similar pairs and prune corresponding tokens in Group A . We prune one token in each selected pair instead of merging them, due to the following reasons: (i) since tokens in the selected pairs are similar, pruning one of them results in minimal information loss; (ii) merged tokens should have higher weights in the following computation [3], which makes it incompatible with certain backbones, such as Sparse Transformer [6]. Finally, we pass the remaining tokens to the next stage. The complexity of **S-stage** is $O(N^2 \times d)$, where N is the number of tokens and d is the dimension of token embeddings.

Importance-guided partitioning in the **S-stage** facilitates stable control over the importance of the pruned tokens for different input images. By pruning similar tokens instead of merging them, our method maintains compatibility with certain specialized backbones [6] while incurring only minimal information loss.

4. Experimental Results

In this section, we first describe the visualized token pruning process of several images in the ImageNet validation dataset, as shown in Fig. 5. We also present ablation experiments to validate our design choices and the effectiveness of our proposed methods. Then, we compare Zero-TPrune with state-of-the-art token pruning methods.

Experimental Setup: To compare different pruning methods, we apply them to various vision Transformer backbones and evaluate the performance of pruned models on ImageNet [9]. We evaluate the models on 224px images unless otherwise noted. We estimate the inference GFLOPS on a V100 GPU using the `fvcore`¹ library. We measure the inference throughput of pruned models on a single A100 GPU and perform fine-tuning after pruning on A100 GPUs.

Although our experiments focus on the classification task, Zero-TPrune can potentially be applied to other tasks, such as generation and segmentation. We refer to the design that can be transferred to other tasks as “**Zero-TPrune-uni**”, meaning “Zero-TPrune for universal purpose.” For the classification task, the CLS token is known to be much more important than other tokens, and its attention weights are a much stronger signal for selecting tokens [14]. Thus, instead of initializing the importance score of tokens uniformly, we assign the CLS token an importance score that is \sqrt{N} times larger than other tokens during initialization in the **I-stage**, where N is the number of tokens. We call this design “**Zero-TPrune**” in the following experiments.

For ablation experiments, we implement Zero-TPrune on the DeiT-S model [36] with different configurations and design choices. For comparisons with state-of-the-art token pruning works, we divide them into two types: (1) methods that require fine-tuning of the pruned model, includ-

ing DynamicViT [30] and A-ViT [43]; (2) fine-tuning-free methods, including ATS [14] and ToMe [3] (which is a token-merging instead of a token-pruning method, but is also fine-tuning-free). For the first type, we compare implementations on DeiT models. We use the official implementation of DynamicViT to reproduce its results and also generate some new ones for comparison. For A-ViT, we directly use the results presented in that article. For the second type, we use the official open-source code of ATS and ToMe to implement them on various pre-trained Transformer backbones, including DeiT [36], LV-ViT [18], MAE [17], AugReg [33], and SWAG [32]. We compare the off-the-shelf performance of Zero-TPrune with theirs. In addition, we compare the performance of pruned models on downstream tasks to check their transfer learning capability, following the selection of datasets in [5]. We provide details of the selected datasets in Supplementary Material Section F. Note that ToMe has an optional design, Proportional Attention (PA), that is dedicated to classification [2] and is not compatible with sparse attention design [6]. We call ToMe with PA disabled “ToMe-uni” and ToMe with PA enabled “ToMe.” ATS is a method solely based on the CLS token; hence, it does not have a universal version.

To further validate the effectiveness of Zero-TPrune, we supplement comparisons with depth-adaptive methods and other straightforward attention-based token ranking methods (e.g., averaging the received attention) in Supplementary Material Section H.1 and H.2.

4.1. Ablation Experiments

We use ablation experiments to determine the optimal hyperparameters for Zero-TPrune. First, it is computationally expensive to check whether the WPR algorithm converges after each iteration. Thus, it would be desirable if we could determine the number of its iterations in advance. By checking the importance distributions after different numbers of iterations and computing the Kullback-Liebler (KL) divergence between them, we find 30-50, 5-10, and 1 iteration(s) are enough to ensure convergence in the first three layers, medium layers, and last three layers, respectively. We provide visual and quantitative comparisons in Supplementary Material Section G.1. Second, we determine good enough minimum and maximum thresholds for VHF through random initialization and greedy search. We provide detailed search configurations and results in Supplementary Material Section G.2. The range found is [0.01,0.7], which is the default setting in our experiments. Third, we explore optimal design choices in the **S-stage** with ablation experiments presented in Supplementary Material Section G.3.

To illustrate the effectiveness of the different techniques employed in Zero-TPrune, we break down their contribution. We apply different combinations of techniques employed in Zero-TPrune to the DeiT-S model and evaluate

¹<https://github.com/facebookresearch/fvcore>



Figure 5. Visualized examples of the pruning process conducted by Zero-TPrune. Images are randomly selected from ImageNet validation dataset. When the pruning rate is aggressive and the main object occupies most of the image area, it is not enough to only prune background tokens. Zero-TPrune exploits similarity between main object tokens and prunes redundant ones.

the performance of the pruned models. We insert pruning layers after the [1,3,6,9,11]-th layer with a retention rate of [1,0.9,0.8,0.7,1] and #iterations of [30,5,5,1,1] in the **I-stage**, and prune 10 tokens in each **S-stage**. Before adding the **S-stage**, we insert pruning layers after the [3,6,9,11]-th layer with a retention rate of [0.8,0.7,0.7,0.6] and #iterations of [5,5,1,1]. We show the results in Table 1 (we provide corresponding results of Zero-TPrune-uni in Supplementary Material Section G.4). The WPR algorithm improves the performance significantly. The EIR/VHF techniques and the **S-stage** improve the performance further.

Table 1. Contribution breakdown of the different techniques employed in Zero-TPrune. The used batch size is 512.

Acc@1	Params	FLOPS/img	Throughput	Method
79.8% (base)	22M	4.55G	1505.9 img/s	Unpruned model
76.8% (-3.0%)	22M	3.08G	2164.4 img/s	random drop
78.6% (+1.8%)	22M	3.08G	2136.5 img/s	WPR
78.8% (+0.2%)	22M	3.08G	2132.6 img/s	WPR+EIR
78.9% (+0.1%)	22M	3.08G	2103.1 img/s	WPR+EIR+VHF (I-stage)
79.4% (+0.5%)	22M	3.08G	2063.9 img/s	I-stage + S-stage

To further improve the performance of pruned models, we can employ Monto Carlo Simulation (MCS) to randomly explore the hyperparameter space, which includes the number and location of pruning layers, corresponding retention rates, number of iterations in each layer, and number of tokens to be pruned in each **S-stage**. After conducting thousands of trials, we select the optimal setting that exhibits the best performance achieved by Zero-TPrune while maintaining a fixed GFLOPS budget. In the case shown in Table 1, MCS helps to achieve 79.5% accuracy with 3.08 GFLOPS. To ensure a fair comparison, we do not use MCS in Zero-TPrune in subsequent comparisons with state-of-the-art methods. Zero-TPrune is not sensitive to the hyperparameter choice, as illustrated with experimental results in Supplementary Material Section G.5.

4.2. Comparison with State-of-the-Art Methods

In this section, we choose the number and location of pruning layers with either constant or uniformly declining retention rates to match the given GFLOPS budget. We keep the

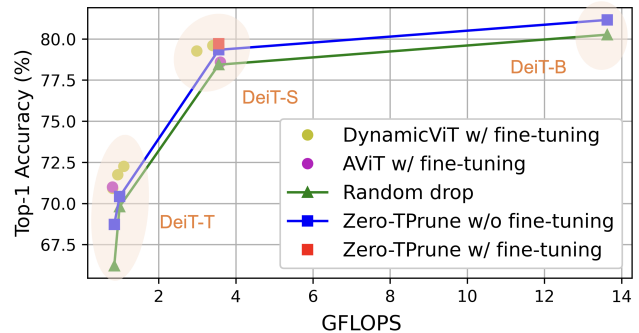


Figure 6. Performance comparison between Zero-TPrune and state-of-the-art fine-tuning-required methods.

number of pruned tokens in each **S-stage** constant. We fix the number of iterations to 30, 5, and 1 for the first three, intermediate, and the last three layers, respectively.

Comparison with Fine-Tuning-Required Methods: To illustrate the advantages of Zero-TPrune, we compare its performance with that of DynamicViT and A-ViT with/without fine-tuning after pruning. Given the random initialization and the fact that the pruning modules in DynamicViT and A-ViT need to be trained, the performance of DynamicViT and A-ViT without fine-tuning after pruning is based on randomly-pruned tokens. Fig. 6 clearly demonstrates the advantages of Zero-TPrune over state-of-the-art fine-tuning-required pruning methods, i.e., DynamicViT and A-ViT. Without fine-tuning after pruning, Zero-TPrune outperforms DynamicViT and A-ViT (using random drop in this case) by around 1%. This means Zero-TPrune **reduces the accuracy drop by more than 60%**. The performance of Zero-TPrune without fine-tuning after pruning is comparable to that of DynamicViT and A-ViT with fine-tuning after pruning (e.g., 0.1% accuracy loss relative to the best, given a 3.5 GFLOPS budget on DeiT-S). With fine-tuning after pruning, Zero-TPrune outperforms both DynamicViT and A-ViT. Zero-TPrune can also be easily applied to larger models (e.g., given a 13.6 GFLOPS budget on DeiT-B) for higher accuracy. On the contrary, applying DynamicViT and A-ViT to large models is very computationally expensive due to their expensive fine-tuning after pruning.

Comparison with Fine-Tuning-Free Methods: ATS and ToMe provide an off-the-shelf option to prune Transformer models without the requirement of fine-tuning after pruning. We first apply them and Zero-TPrune to the DeiT-S model to compare off-the-shelf performance after pruning without fine-tuning. The results are shown in Fig. 7 and Table 2. We provide more results related to throughput in Supplementary Material Section H.3. As shown in Fig. 7, compared with state-of-the-art fine-tuning-free methods, Zero-TPrune **reduces the accuracy loss by 33%** on the DeiT-S model with a 3 GFLOPS budget. If we change the pruning configuration and give a lower budget (e.g., reduce GFLOPS by 45%), the accuracy loss introduced by Zero-TPrune is still only 0.7%. Zero-TPrune can **reduce GFLOPS by 13% at nearly no cost**. Note that these results are obtained without fine-tuning.

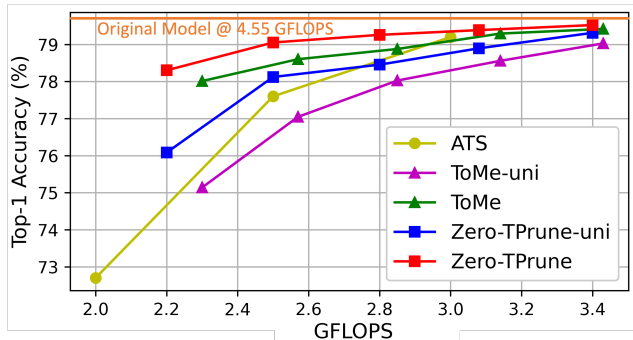


Figure 7. Performance comparison between Zero-TPrune and state-of-the-art fine-tuning-free methods. The applied Transformer backbone is DeiT-S.

Table 2. Performance of pruned DeiT-S models without fine-tuning. Throughput is measured on a single NVIDIA A100 GPU.

Method	Acc@top1	GFLOPS	Throughput(img/s)
DeiT-S	79.8%	4.55	1505.9
+ ATS	79.2% (-0.6%)	3.00 (-33.4%)	2062.3 (+36.9%)
+ ToMe	78.9% (-0.9%)	2.95 (-35.2%)	2263.9 (+50.3%)
+ Zero-TP-a	79.4% (-0.4%)	2.97 (-34.7%)	2188.4 (+45.3%)
+ Zero-TP-b	79.1% (-0.7%)	2.50 (-45.1%)	2458.4 (+63.2%)
+ Zero-TP-c	79.8% (-0.0%)	3.97 (-12.7%)	1673.2 (+11.1%)

We further evaluate Zero-TPrune and baselines on various backbones with different sizes. The results are shown in Table 3. We find that when the original model is medium-sized, e.g., AugReg and LV-ViT-S, Zero-TPrune outperforms baseline methods by a large margin (it reduces accuracy loss by up to 49%). For large models, if the pruning is moderate (i.e., reduce GFLOPS by 20%), Zero-TPrune still outperforms baseline methods. However, we found when large models are aggressively pruned (i.e., reduce GFLOPS by 50%), Zero-TPrune does not outperform baselines. Note that aggressively pruning large models is usually not a good idea, which is indicated by comparing the optimal pruned LV-ViT-M model (*ToMe*, 81.6% with 6.3 GFLOPS) and the optimal pruned LV-ViT-S model (*Zero-TPrune*, 81.5%

with 3.5 GFLOPS). The latter requires only 60% of the GFLOPS at the cost of 0.1% accuracy loss. Compared with aggressively-pruned large models, using a smaller pre-trained model instead is often a better choice. We provide a detailed discussion in Supplementary Material Section I.

We also evaluate the performance of pruned models on downstream tasks to measure their transfer learning capability. We select several small image datasets for this purpose. Zero-TPrune outperforms baselines on most datasets, indicating its strong transfer learning capability after pruning. We introduce selected datasets and present detailed experimental results in Supplementary Material Section F.

Table 3. Performance of pruned AugReg, LV-ViT, and SWAG models without fine-tuning. SWAG models perform inference on 384px images.

Method	Acc@top1	GFLOPS	Method	Acc@top1	GFLOPS
AugReg	81.41%	4.55	MAE	83.62%	55.4
+ ATS	79.21%	2.80	+ATS	82.07%	42.3
+ ToMe	79.30%	2.78	+ToMe	82.69%	42.2
+ Zero-TP	80.22%	2.79	+Zero-TP	82.93%	42.3
LV-ViT-S	83.3%	6.6	SWAG	85.30%	55.6
+ ATS	80.4%	3.5	+ATS	84.21%	43.8
+ ToMe	79.8%	3.6	+ToMe	85.09%	43.8
+ Zero-TP	81.5%	3.5	+Zero-TP	85.17%	43.8

5. Conclusion

In this article, we proposed Zero-TPrune, a zero-shot token pruning method that exploits both the importance and similarity of tokens to eliminate the fine-tuning process for pruning. In the **I-stage**, it considers the attention matrix to be an adjacency matrix of an attention graph, which reduces noise from unimportant tokens. In the **S-stage**, it uses importance distribution to guide token partitioning and similarity-based pruning, making them more stable and precise. Through the implementation of Zero-TPrune and baseline methods on various Transformer backbones and evaluation on ImageNet, we showed that it can eliminate the fine-tuning process for pruning with very small accuracy reduction. Moreover, when compared to state-of-the-art off-the-shelf pruning methods, Zero-TPrune not only outperforms them by reducing accuracy loss by up to 49% but also enhances the transfer learning capability of pruned models. These findings emphasize the effectiveness of Zero-TPrune in balancing model compression and preservation of performance, making it a promising approach for efficient and accurate pruning of Transformer models. Future work can enhance the capabilities of Zero-TPrune further. One intriguing topic of future study is examining the applicability of Zero-TPrune on tasks such as image reconstruction, segmentation, and generation. Investigating the potential benefits and efficiency gains of employing Zero-TPrune in these domains holds promise for advancing the field further. **Acknowledgment.** This work was supported by NSF under Grant No. CCF-2203399.

References

- [1] Andrea Banino, Jan Balaguer, and Charles Blundell. PonderNet: Learning to Ponder. *arXiv preprint arXiv:2107.05407*, 2021.
- [2] Daniel Bolya and Judy Hoffman. Token Merging for Fast Stable Diffusion. In *Proceedings of the IEEE/CVF Conference on Computer Vision and Pattern Recognition*, pages 4598–4602, 2023.
- [3] Daniel Bolya, Cheng-Yang Fu, Xiaoliang Dai, Peizhao Zhang, Christoph Feichtenhofer, and Judy Hoffman. Token Merging: Your ViT But Faster. *arXiv preprint arXiv:2210.09461*, 2022.
- [4] Sergey Brin. The PageRank Citation Ranking: Bringing Order to the Web. *Proceedings of ASIS, 1998*, 98:161–172, 1998.
- [5] Yun-Hao Cao, Hao Yu, and Jianxin Wu. Training Vision Transformers with Only 2040 Images. In *Proceedings of the European Conference on Computer Vision*, pages 220–237. Springer, 2022.
- [6] Rewon Child, Scott Gray, Alec Radford, and Ilya Sutskever. Generating Long Sequences with Sparse Transformers. *arXiv preprint arXiv:1904.10509*, 2019.
- [7] Mircea Cimpoi, Subhansu Maji, Iasonas Kokkinos, Sammy Mohamed, and Andrea Vedaldi. Describing Textures in the Wild. In *Proceedings of the IEEE Conference on Computer Vision and Pattern Recognition*, pages 3606–3613, 2014.
- [8] Marco Cuturi, Olivier Teboul, and Jean-Philippe Vert. Differentiable Ranking and Sorting Using Optimal Transport. *Advances in Neural Information Processing Systems*, 32, 2019.
- [9] Jia Deng, Wei Dong, Richard Socher, Li-Jia Li, Kai Li, and Li Fei-Fei. ImageNet: A Large-Scale Hierarchical Image Database. In *Proceedings of the IEEE Conference on Computer Vision and Pattern Recognition*, pages 248–255, 2009.
- [10] Jacob Devlin, Ming-Wei Chang, Kenton Lee, and Kristina Toutanova. BERT: Pre-Training of Deep Bidirectional Transformers for Language Understanding. *arXiv preprint arXiv:1810.04805*, 2018.
- [11] Peiyan Dong, Mengshu Sun, Alec Lu, Yanyue Xie, Kenneth Liu, Zhenglun Kong, Xin Meng, Zhengang Li, Xue Lin, Zhenman Fang, et al. HeatViT: Hardware-Efficient Adaptive Token Pruning for Vision Transformers. In *Proceedings of the IEEE International Symposium on High-Performance Computer Architecture*, pages 442–455, 2023.
- [12] Alexey Dosovitskiy, Lucas Beyer, Alexander Kolesnikov, Dirk Weissenborn, Xiaohua Zhai, Thomas Unterthiner, Mostafa Dehghani, Matthias Minderer, Georg Heigold, Sylvain Gelly, et al. An Image is Worth 16x16 Words: Transformers for Image Recognition at Scale. *arXiv preprint arXiv:2010.11929*, 2020.
- [13] Maha Elbayad, Jiatao Gu, Edouard Grave, and Michael Auli. Depth-Adaptive Transformer. *arXiv preprint*, 2019.
- [14] Mohsen Fayyaz, Soroush Abbasi Koohpayegani, Farnoush Rezaei Jafari, Sunando Sengupta, Hamid Reza Vaezi Joze, Eric Sommerlade, Hamed Pirsiavash, and Jürgen Gall. Adaptive Token Sampling for Efficient Vision Transformers. In *Proceedings of the European Conference on Computer Vision*, pages 396–414. Springer, 2022.
- [15] Saurabh Goyal, Anamitra Roy Choudhury, Saurabh Raje, Venkatesan Chakaravarthy, Yogish Sabharwal, and Ashish Verma. PoWER-BERT: Accelerating BERT Inference via Progressive Word-Vector Elimination. In *Proceedings of the International Conference on Machine Learning*, pages 3690–3699. PMLR, 2020.
- [16] Alex Graves. Adaptive Computation Time for Recurrent Neural Networks. *arXiv preprint arXiv:1603.08983*, 2016.
- [17] Kaiming He, Xinlei Chen, Saining Xie, Yanghao Li, Piotr Dollár, and Ross Girshick. Masked Autoencoders are Scalable Vision Learners. In *Proceedings of the IEEE/CVF Conference on Computer Vision and Pattern Recognition*, pages 16000–16009, 2022.
- [18] Zi-Hang Jiang, Qibin Hou, Li Yuan, Daquan Zhou, Yujun Shi, Xiaojie Jin, Anran Wang, and Jiashi Feng. All Tokens Matter: Token Labeling for Training Better Vision Transformers. *Advances in Neural Information Processing Systems*, 34:18590–18602, 2021.
- [19] Gyuwan Kim and Kyunghyun Cho. Length-Adaptive Transformer: Train Once with Length Drop, Use Anytime with Search. *arXiv preprint arXiv:2010.07003*, 2020.
- [20] Sehoon Kim, Sheng Shen, David Thorsley, Amir Gholami, Woosuk Kwon, Joseph Hassoun, and Kurt Keutzer. Learned Token Pruning for Transformers. In *Proceedings of the 28th ACM SIGKDD Conference on Knowledge Discovery and Data Mining*, pages 784–794, 2022.
- [21] Zhenglun Kong, Peiyan Dong, Xiaolong Ma, Xin Meng, Wei Niu, Mengshu Sun, Xuan Shen, Geng Yuan, Bin Ren, Hao Tang, et al. SPViT: Enabling Faster Vision Transformers Latency-Aware Soft Token Pruning. In *Proceedings of the European Conference on Computer Vision*, pages 620–640. Springer, 2022.
- [22] Jonathan Krause, Michael Stark, Jia Deng, and Li Fei-Fei. 3D Object Representations for Fine-Grained Categorization. In *Proceedings of the IEEE International Conference on Computer Vision Workshops*, pages 554–561, 2013.
- [23] Weijie Liu, Peng Zhou, Zhe Zhao, Zhiruo Wang, Haotang Deng, and Qi Ju. FastBERT: a Self-Distilling BERT with Adaptive Inference Time. *arXiv preprint arXiv:2004.02178*, 2020.
- [24] Xiangcheng Liu, Tianyi Wu, and Guodong Guo. Adaptive Sparse ViT: Towards Learnable Adaptive Token Pruning by Fully Exploiting Self-Attention. *arXiv preprint arXiv:2209.13802*, 2022.
- [25] Subhansu Maji, Esa Rahtu, Juho Kannala, Matthew Blaschko, and Andrea Vedaldi. Fine-Grained Visual Classification of Aircraft. *arXiv preprint arXiv:1306.5151*, 2013.
- [26] Volodymyr Mnih, Koray Kavukcuoglu, David Silver, Andrei A. Rusu, Joel Veness, Marc G. Bellemare, Alex Graves, Martin Riedmiller, Andreas K. Fidjeland, Georg Ostrovski, et al. Human-Level Control through Deep Reinforcement Learning. *Nature*, 518(7540):529–533, 2015.
- [27] Maria-Elena Nilsback and Andrew Zisserman. A Visual Vocabulary for Flower Classification. In *Proceedings of the IEEE Computer Society Conference on Computer Vision and Pattern Recognition*, pages 1447–1454, 2006.

- [28] Omkar M. Parkhi, Andrea Vedaldi, Andrew Zisserman, and C.V. Jawahar. Cats and Dogs. In *Proceedings of the IEEE Conference on Computer Vision and Pattern Recognition*, pages 3498–3505, 2012.
- [29] Ariadna Quattoni and Antonio Torralba. Recognizing Indoor Scenes. In *Proceedings of the IEEE Conference on Computer Vision and Pattern Recognition*, pages 413–420, 2009.
- [30] Yongming Rao, Wenliang Zhao, Benlin Liu, Jiwen Lu, Jie Zhou, and Cho-Jui Hsieh. DynamicViT: Efficient Vision Transformers with Dynamic Token Sparsification. *Advances in Neural Information Processing Systems*, 34:13937–13949, 2021.
- [31] Stefan Schaal and Christopher G. Atkeson. Learning Control in Robotics. *IEEE Robotics & Automation Magazine*, 17(2): 20–29, 2010.
- [32] Mannat Singh, Laura Gustafson, Aaron Adcock, Vinicius de Freitas Reis, Bugra Gedik, Raj Prateek Kosaraju, Dhruv Mahajan, Ross Girshick, Piotr Dollár, and Laurens Van Der Maaten. Revisiting Weakly Supervised Pre-Training of Visual Perception Models. In *Proceedings of the IEEE/CVF Conference on Computer Vision and Pattern Recognition*, pages 804–814, 2022.
- [33] Andreas Steiner, Alexander Kolesnikov, Xiaohua Zhai, Ross Wightman, Jakob Uszkoreit, and Lucas Beyer. How to Train Your ViT? Data, Augmentation, and Regularization in Vision Transformers. *arXiv preprint arXiv:2106.10270*, 2021.
- [34] Christian Szegedy, Wojciech Zaremba, Ilya Sutskever, Joan Bruna, Dumitru Erhan, Ian Goodfellow, and Rob Fergus. Intriguing Properties of Neural Networks. *arXiv preprint arXiv:1312.6199*, 2013.
- [35] Quan Tang, Bowen Zhang, Jiajun Liu, Fagui Liu, and Yifan Liu. Dynamic Token Pruning in Plain Vision Transformers for Semantic Segmentation. In *Proceedings of the IEEE/CVF International Conference on Computer Vision*, pages 777–786, 2023.
- [36] Hugo Touvron, Matthieu Cord, Matthijs Douze, Francisco Massa, Alexandre Sablayrolles, and Hervé Jégou. Training Data-Efficient Image Transformers & Distillation through Attention. In *Proceedings of the International Conference on Machine Learning*, pages 10347–10357. PMLR, 2021.
- [37] Ashish Vaswani, Noam Shazeer, Niki Parmar, Jakob Uszkoreit, Llion Jones, Aidan N. Gomez, Łukasz Kaiser, and Illia Polosukhin. Attention is All You Need. *Advances in Neural Information Processing Systems*, 30, 2017.
- [38] Catherine Wah, Steve Branson, Peter Welinder, Pietro Perona, and Serge Belongie. The Caltech-UCSD Birds-200-2011 Dataset. *California Institute of Technology*, https://www.vision.caltech.edu/datasets/cub_200_2011/, 2011.
- [39] Hanrui Wang, Zhekai Zhang, and Song Han. SpAtten: Efficient Sparse Attention Architecture with Cascade Token and Head Pruning. In *Proceedings of the IEEE International Symposium on High-Performance Computer Architecture*, pages 97–110, 2021.
- [40] Siyuan Wei, Tianzhu Ye, Shen Zhang, Yao Tang, and Jiajun Liang. Joint Token Pruning and Squeezing Towards More Aggressive Compression of Vision Transformers. In *Proceedings of the IEEE/CVF Conference on Computer Vision and Pattern Recognition*, pages 2092–2101, 2023.
- [41] Xiaohua Zhai, Alexander Kolesnikov, Neil Houlsby, and Lucas Beyer. Scaling Vision Transformers. In *Proceedings of the IEEE/CVF Conference on Computer Vision and Pattern Recognition*, pages 12104–12113, 2022.
- [42] Deming Ye, Yankai Lin, Yufei Huang, and Maosong Sun. Tr-BERT: Dynamic Token Reduction for Accelerating BERT Inference. *arXiv preprint arXiv:2105.11618*, 2021.
- [43] Hongxu Yin, Arash Vahdat, Jose M. Alvarez, Arun Mallya, Jan Kautz, and Pavlo Molchanov. A-ViT: Adaptive Tokens for Efficient Vision Transformer. In *Proceedings of the IEEE/CVF Conference on Computer Vision and Pattern Recognition*, pages 10809–10818, 2022.

Zero-TPrune: Zero-Shot Token Pruning through Leveraging of the Attention Graph in Pre-Trained Transformers

Supplementary Material

A. The I-S Pattern and the I'-S-I Pattern

In this section, we first demonstrate the *overwhelming of the major group* issue caused by the I-S pattern and then compare it with the I'-S-I pattern visually.

A.1. Overwhelming of the Major Group with the I-S Pattern

Sometimes, unimportant parts of an image may be identified as important and important parts as unimportant by our graph-based WPR algorithm. In the **I-stage**, each token votes for "more important tokens" and the weight of their votes is determined by their importance in the last round of voting. Besides the semantically significant tokens, tokens also intend to vote for tokens *that are similar to them*. When semantically significant tokens (e.g., main object tokens) are only a small part of an image and unimportant background tokens dominate, sometimes background tokens vote for each other and gradually obtain high importance scores after multiple rounds of voting. An example is shown in Fig. 8. It shows that the background of the image is considered important in the Transformer heads. The fish itself, surprisingly, is considered unimportant.

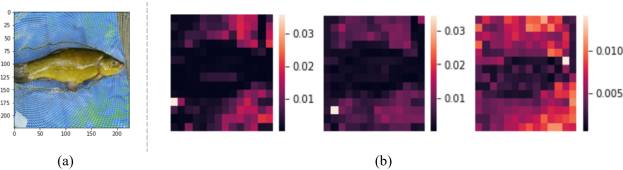


Figure 8. An example illustrating that a large unimportant group may overwhelm a small important group: (a) input image and (b) three examples showing that unimportant background tokens overwhelm the important fish tokens.

In this image, the *background* and *fish* tokens form two sets: *A* and *B*. In the beginning, because tokens in *set B* are more semantically significant than those in *set A*, they have relatively high importance scores. However, both tokens in *set A* and *set B* mainly intend to vote for tokens in their own set. Thus, it is easier for *set A* to form tokens with high importance scores because *set A* includes more tokens. These "highly important" tokens have larger voting weights in the next iteration. This makes it even easier for other tokens in *set A* to get "high importance." This is a positive feedback loop, with the result that the most "important" tokens end up in *set A*.

A.2. Comparison

As shown in Fig. 9, by pruning similar background tokens in advance, the *overwhelming of the major group* problem is alleviated significantly.

B. Attention Probability Matrix

ViT [12] and its variants contain multiple Transformer encoder layers that are stacked up together. The basic Transformer encoder layer includes a multi-head attention (MHA) block followed by a feed-forward network (FFN) block, with residual connections and layer normalization around each. We make the assumption that an MHA block consists of H independently parameterized heads. An attention head h in layer l can be parameterized by the Key, Query, and Value weight matrices: $\mathbf{W}_k^{(h,l)}, \mathbf{W}_q^{(h,l)}, \mathbf{W}_v^{(h,l)} \in \mathbb{R}^{d_h \times d}$, and the output weight matrix $\mathbf{W}_o^{(h,l)} \in \mathbb{R}^{d \times d_h}$, where d_h is typically set to d/H and d is the embedded feature dimension. Suppose $x \in \mathbb{R}^{d \times n}$ is the input sequence and n is the input sequence length. For each head, the *attention probability* between token x_i and x_j is given as an element of matrix $\mathbf{A}^{(h,l)}$:

$$\mathbf{A}^{(h,l)}(x_i, x_j) = \text{softmax}_{(i,j)} \left(\frac{x_i^T \mathbf{W}_q^T \mathbf{W}_k x_j}{\sqrt{d}} \right) \in \mathbb{R} \quad (3)$$

This matrix measures how much token x_j attends to token x_i . The output of an MHA block can be formulated as follows:

$$x_{\text{MHA}} = \text{LN} \left(\mathbf{W}_o \sum_{i=1}^n \mathbf{W}_v x_i \mathbf{A}^{(h,l)}(x_i, x_j) + x \right) \quad (4)$$

The output of a Transformer encoder layer can be formulated as follows:

$$x_{\text{out}} = \text{LN} (\sigma (\mathbf{W}_2 (\mathbf{W}_1 x_{\text{MHA}} + b_1)) + b_2 + x_{\text{MHA}}) \quad (5)$$

where $\mathbf{W}_1, \mathbf{W}_2, b_1$, and b_2 are FFN parameters, and σ and LN denote the activation function and layer normalization, respectively. We can see that the computation overhead of a Transformer encoder layer undergoes a quadratic reduction when tokens are pruned.

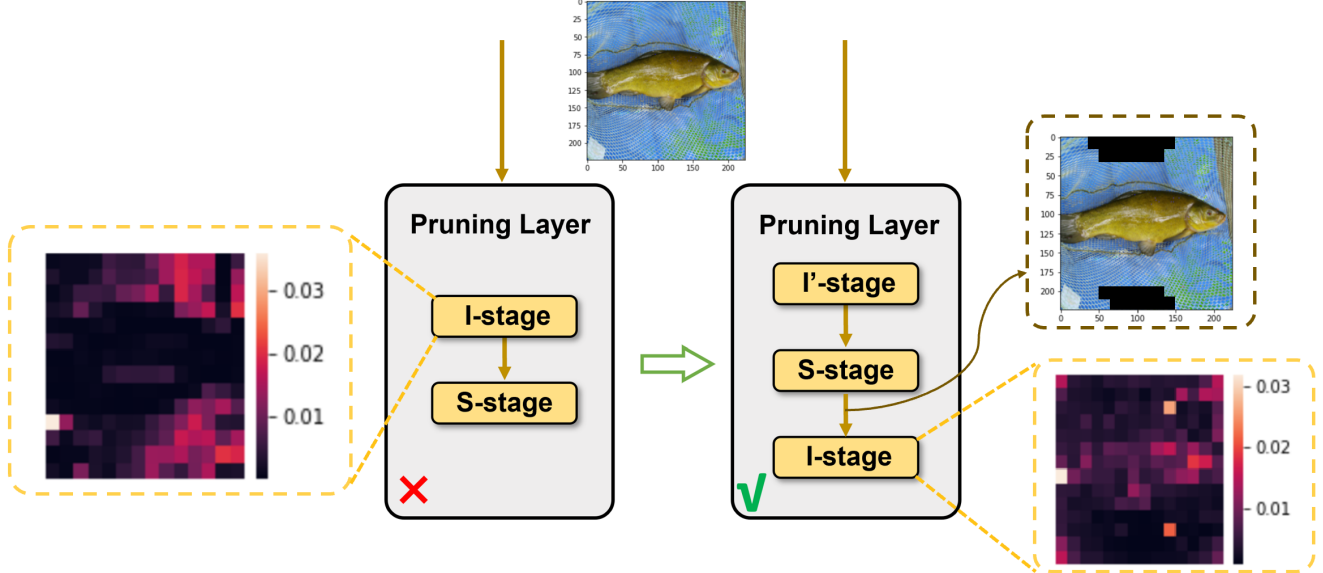


Figure 9. Visual comparison between the I-S pattern and the I'-S-I pattern.

C. Optional Training Paradigm after Pruning

Zero-TPrune can eliminate the fine-tuning process after pruning with a very small accuracy reduction. However, in some scenarios, we may have adequate samples and computational resources. In such cases, the performance of Zero-TPrune can be improved further by training (fine-tuning) after pruning. In this section, we introduce techniques used to accomplish this.

Given that it is very expensive to make importance-based ranking differentiable [8], we eliminate the **S-stage** and retain only the **I-stage** when we aim to further train (fine-tune) the pruned model. Besides this, to make Zero-TPrune differentiable, it is necessary to replace normal token pruning with “soft token pruning.” Instead of completely discarding pruned tokens, soft token pruning assigns them small weights to reduce their effect on later computation and preserves compatibility with back-propagation during training. In this way, the non-differentiable token mask M is replaced with a differentiable soft mask \tilde{M} using the sigmoid operation:

$$\tilde{M}^{(l)}(x_i) = \sigma\left(\frac{s^{(l)}(x_i) - \theta^{(l)}}{T}\right) \quad (6)$$

where $s^{(l)}(x_i)$ is the importance score of token x_i and $\theta^{(l)}$ is the importance threshold for the l -th layer. $\theta^{(l)}$ is determined based on the chosen pruning rate and GFLOPS budget. Details of soft token pruning can be found in [20].

For simplicity, we use a similar loss function to DynamicViT [30], which includes three terms:

$$\mathcal{L} = \mathcal{L}_{\text{cls}} + \lambda_{\text{distill}} \mathcal{L}_{\text{distill}} + \lambda_{\text{KL}} \mathcal{L}_{\text{KL}} \quad (7)$$

The first term is the standard classification cross-entropy loss:

$$\mathcal{L}_{\text{cls}} = \text{CrossEntropy}(y, \bar{y}) \quad (8)$$

During fine-tuning, we use the original backbone network as the teacher model and push the behavior of the Zero-TPrune model to be as close to the teacher model as possible. First, we push the finally retained tokens of Zero-TPrune close to the ones of the teacher model. This contributes to the second distillation term above. We also minimize the difference in predictions between Zero-TPrune and its teacher via Kullback-Liebler (KL) divergence. This contributes to the third term. Details of the loss function can be found in [30].

D. Visualization

In this section, we use some visualization examples to provide high-level insights.

D.1. An Input Image Example

Fig. 10 shows a simple test sample of a *fish* from the ImageNet dataset and the corresponding importance score distributions in different layers and heads. We can see that most heads can successfully capture the important part of this image with the help of the graph-based WPR algorithm.

D.2. Averaged Importance Distribution over Thousands of Images

Another interesting visualization example is related to the general functionality of different layers in the Transformers.

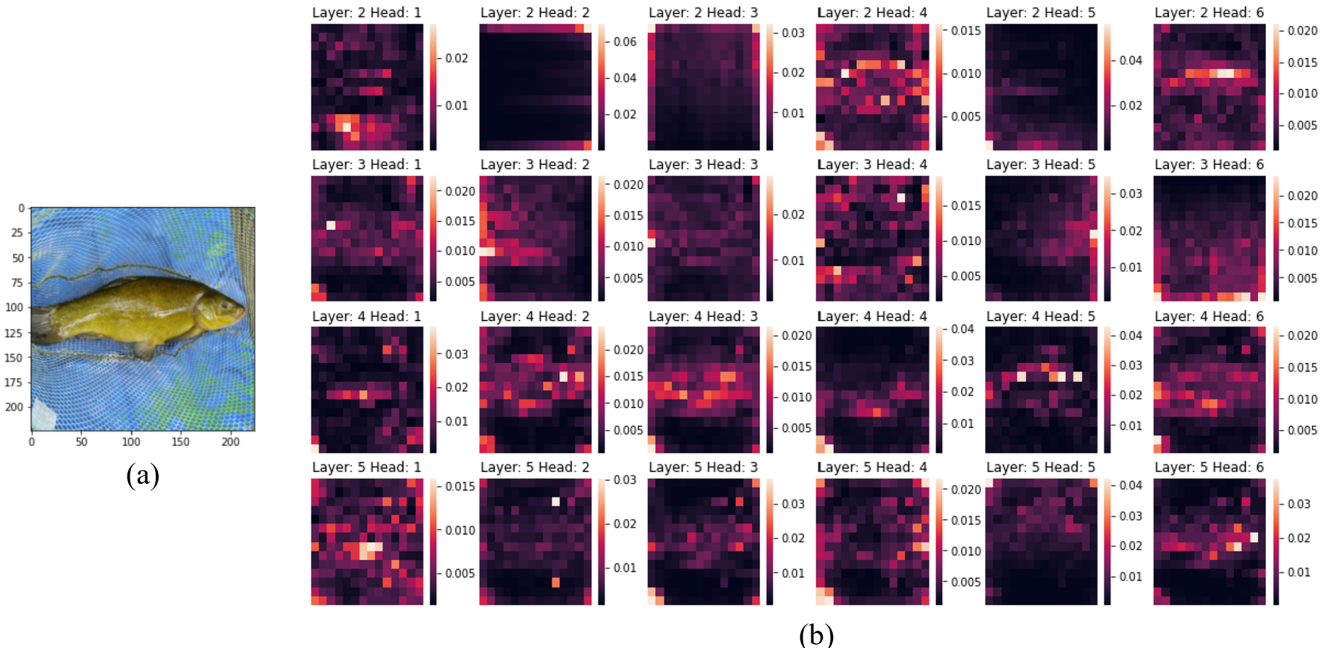


Figure 10. The important part of input images can be successfully captured by the graph-based WPR algorithm: (a) a test sample of *fish* in the ImageNet dataset and (b) the corresponding importance score distributions given by the WPR algorithm in different layers. The used backbone is DeiT-S.

Fig. 11 shows the importance score distributions averaged over thousands of images. It indicates that different layers of the Transformer behave differently. Shallow layers focus more on the edge of input images and deep layers focus more on the center.

E. Combining Results of Different Heads

In this section, we introduce the techniques we propose to nontrivially combine the importance score distribution of different heads from the WPR algorithm.

E.1. Emphasizing Informative Region

Different heads in an encoder layer usually pay attention to different parts of the input image, as shown in Fig. 12. For the input image of a boy holding a fish, some heads pay more attention to the body of this boy, some to the head of this boy, and some to the fish in hand.

We propose EIR to address this issue. Suppose there are three heads in all and the importance scores of tokens A , B , and C are $[9,9,9]$, $[9,0,0]$, $[3,3,3]$, respectively. The ideal importance order is $A > B > C$. Table 4 shows the outcome of application of different importance score calculation methods. The traditional averaging method assigns the same importance to tokens A and B . If we only select the highest score across all heads, tokens A and B will be assigned the same importance, which is also not desired. The proposed EIP technique balances the two situations and re-

Table 4. Application of different importance score calculation methods to the example.

Importance Score	Average $\{S_i\}$	$\max\{S_i\}$	EIP
Token A	9	9	5.2
Token B	3	9	3
Token C	3	3	1.7
Rank	$A > B = C$	$A = B > C$	$A > B > C$

sults in the ideal importance order.

E.2. Variance-based Head Filter

The importance scores given by the WPR algorithm may converge to an undesired distribution. Two typical examples are shown in Fig. 13. Tokens at the edge of the input image get very high importance scores in Fig. 13(b) and the importance score distribution in Fig. 13(c) is nearly uniform. We introduce VHF to mitigate the negative impact of these heads.

F. Downstream Tasks

Table 5 shows the number of categories and test instances in the selected datasets. DTD is a describable textures dataset; Indoor67 is an indoor scene recognition dataset; CUB200 is a challenging dataset of 200 bird species. The other datasets have self-explanatory names.

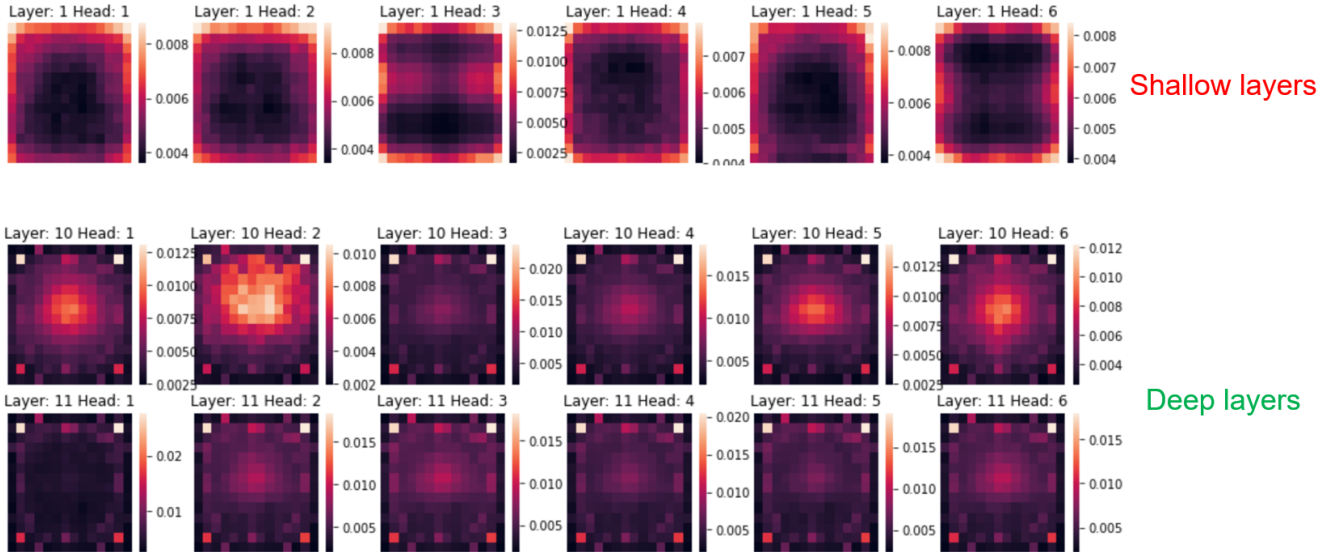


Figure 11. Importance score distributions averaged over thousands of images. The first row is derived from the first layer and the second (third) row from the 10th (11th) layer of the DeiT-S model.

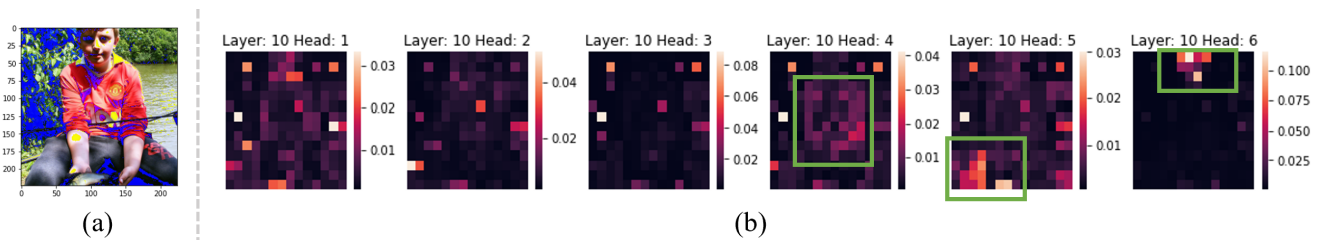


Figure 12. The distribution of importance score from different heads for an input image: (a) an image of a boy holding a fish and (b) importance score distributions. The results are obtained by the WPR algorithm with 30 iterations in the tenth layer of the DeiT-S model.

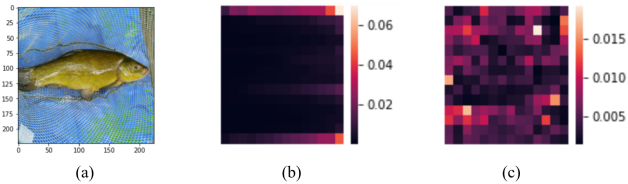


Figure 13. Examples of undesired importance score distributions in certain heads obtained by the WPR algorithm: (a) input image, (b) second head in the second layer of the DeiT-S model, and (c) fourth head in the third layer of the DeiT-S model.

Table 5. Datasets for downstream image classification.

Datasets	#Categories	#Test Instances
Flowers [27]	102	6149
Pets [28]	37	3669
DTD [7]	47	1880
Indoor67 [29]	67	1340
CUB200 [38]	200	5794
Aircrafts [25]	100	3333
Cars [22]	196	8041

G. Ablation Experiments

The experimental results are shown in Table 6. Zero-TPPrune outperforms baselines on most datasets, indicating its strong transfer learning capability after pruning. ToMe has worse performance on small-sized models due to a lack of enough layers to merge tokens gradually.

In this section, we show results for further ablation experiments we performed. We explore the convergence speed of WPR and determine the appropriate number of iterations for each layer in Section G.1. Then we identify a good enough variance threshold for VHF in Section G.2. Furthermore, we describe optimal design choices in the **S-stage** in Sec-

Table 6. Performance of pruned models on downstream tasks.

Model	GFLOPS	Flowers	Pets	DTD	Indoor67	CUB200	Aircrafts	Cars
DeiT-T	1.26	97.3	88.6	73.2	75.6	76.8	78.7	90.3
+ ATS	0.90	94.6	86.1	71.0	72.9	73.8	76.0	88.4
+ ToMe	0.90	93.2	84.7	69.9	71.6	72.9	75.2	87.1
+ Zero-TP	0.91	95.1	86.9	70.9	73.7	74.4	76.7	88.2

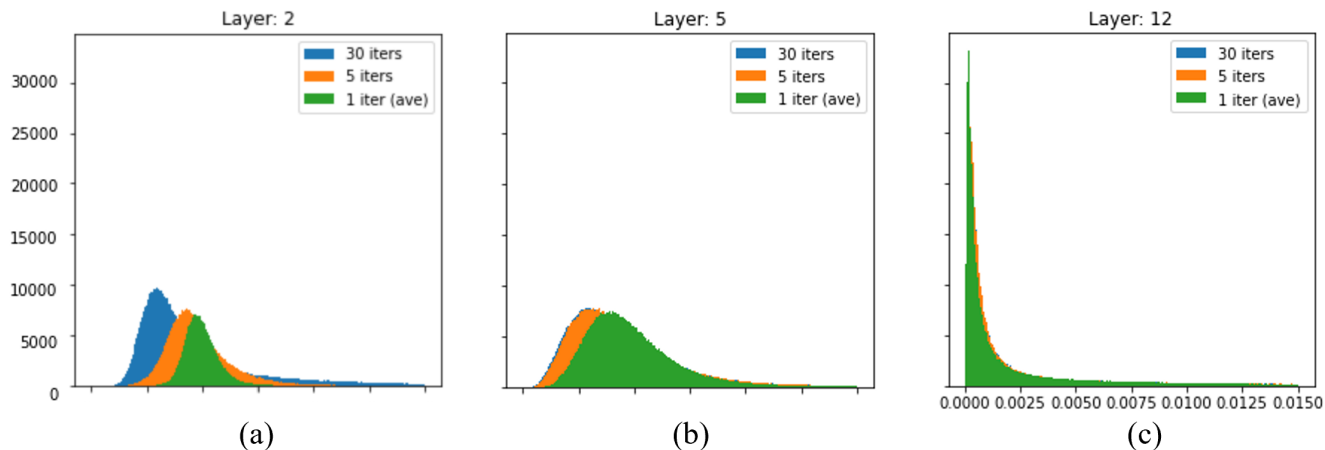


Figure 14. The importance score distributions of tokens in 2,560 images. The distribution changes with both the number of iterations and layer location: (a) layer 2, (b) layer 5, and (c) layer 12 in DeiT-S.

tion G.3, demonstrate the performance of Zero-TP prune-uni in Section G.4, and discuss hyperparameter search in Section G.5.

G.1. Convergence Speed of the WPR Algorithm

It is computationally expensive to check whether the WPR algorithm converges after each iteration. Thus, it would be desirable if we could determine the number of its iterations in advance. In order to do so, we need to derive the general convergence behavior of the WPR algorithm. Fig. 14 shows the importance score distributions of tokens in 2,560 images. In the shallow layers, such as the first layer, the distributions corresponding to 30 iterations and five iterations are obviously different. This indicates that five iterations are not enough to make the WPR algorithm converge in the shallow layers. On the other hand, in the deep layers, such as the 12th layer, the distribution corresponding to 30 iterations is quite similar to the distribution corresponding to just one iteration. This means that one iteration is enough to make the WPR algorithm converge in the deep layers. In addition, in the fifth layer, five iterations are enough to make it converge.

To quantitatively verify the assertions we made above, we calculate the KL divergence between the importance distribution given by 30, 5, 1 iteration(s) and that given by 50 iterations in different layers. The results are shown in

Fig. 15. Thus, to ensure convergence, we set the number of iterations to 30-50, 5-10, and 1 in the first three layers, medium layers, and last three layers, respectively. Another interesting thing to note is that the Transformer model and the WPR algorithm assign low-importance scores to most tokens in the deep layers.

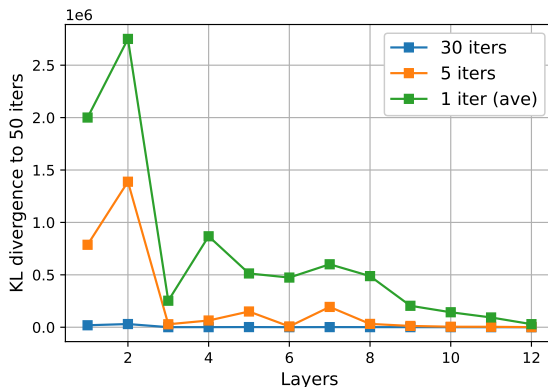


Figure 15. The KL divergence between the importance score distribution given by different numbers of iterations and that given by 50 iterations in different layers. The used backbone is DeiT-S.

G.2. Variance Thresholds for VHF

To exclude noise from heads that converge to undesired importance score distributions (as shown in Fig. 13), we propose VHF and set minimum and maximum thresholds for the variance of head distributions. We perform an ablation experiment to determine the optimal variance range. The pruning configuration is shown in Table 7. We then use random initialization and beam search ($k = 2$) to find a good enough variance range setting. The results are shown in Fig. 16, which points to the range $[0.01, 0.7]$.

Table 7. Pruning configuration used to search for optimal variance thresholds.

Pruning Layers	0	2	4	6	8	10
Retention Rates	0.9	0.9	0.85	0.8	0.7	0.65
# Iterations	50	50	5	5	1	1

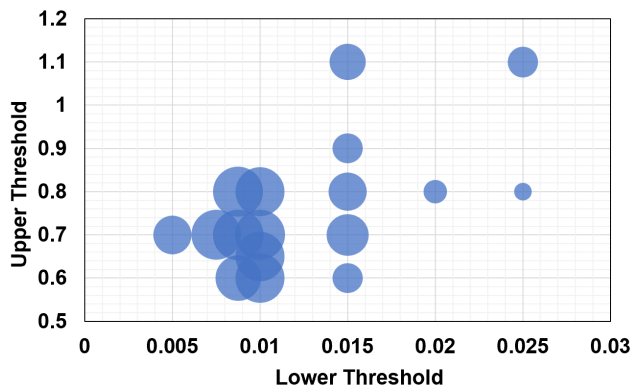


Figure 16. Results obtained in the process of searching for optimal thresholds. A larger blue bubble represents higher accuracy with that setting.

G.3. Optimal Design Choices in the S-stage

As discussed in Section 3.3, the design space of the **S-stage** is composed of three dimensions: (1) source of feature vectors, (2) partitioning method, and (3) similarity metric. We find that the optimal choice is (1) key matrix, (2) sequential (prune unimportant part), and (3) cosine similarity, respectively. This is the default setting in the following experiments unless otherwise noted. For the results in this section, pruning layers are inserted after the $[1, 3, 6, 9, 11]$ -th layer with a retention rate of $[1, 0.9, 0.8, 0.7, 1]$ and #iterations of $[30, 5, 5, 1, 1]$ in the **I-stage**, and 10 tokens are pruned in each **S-stage**. Note that all results in this subsection are augmented by the CLS token by assigning it an importance score that is \sqrt{N} times larger than other tokens during initialization in the **I-stage**, where N is the number of tokens.

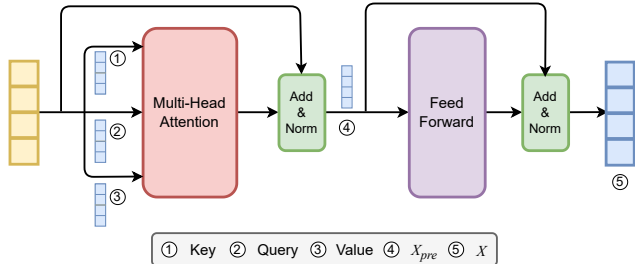


Figure 17. Potential feature vectors that can be used to represent tokens.

Table 8. Ablation experiment results for the source of **feature vectors**.

Feature	Acc@top1	GFLOPS
X_{pre}	79.113%	3.08
X	79.082%	3.08
K	79.351%	3.08
Q	79.205%	3.08
V	79.097%	3.08

Feature vectors: As shown in Fig. 17, feature vectors that represent tokens can be the corresponding vectors in the Key matrix, Query matrix, Value matrix, intermediate embedding vectors in the X_{pre} matrix, or output embedding vectors in the X matrix. We maintain the other settings and change the feature vectors used. The performance of pruned models is shown in Table 8. It indicates that the Key matrix is the optimal source of feature vectors.

Partitioning method: After ranking tokens according to their importance (e.g., $token \{1, 2, 3, 4, 5, 6\}$; $token 1$ has the highest score and $token 6$ has the lowest), we choose from the following options: (i) **Alternate:** alternatively assign them to Group A and B, then the average token importance in two groups is nearly equal (e.g., $A : \{2, 4, 6\}$, $B : \{1, 3, 5\}$); (ii) **Sequential-U:** assign the less important half of tokens to Group A and the other half to Group B, which means we sequentially partition tokens and prune the unimportant part (e.g., $A : \{4, 5, 6\}$, $B : \{1, 2, 3\}$); (iii) **Sequential-I:** assign the more important half of tokens to Group A and the other half to Group B, which means we sequentially partition tokens and prune the important part (e.g., $A : \{1, 2, 3\}$, $B : \{4, 5, 6\}$), (iv) **Random:** randomly assign them to Group A or B; and (v) **No partition:** assign all tokens to both groups without partitioning. To evaluate the effectiveness of these options, we conducted experiments while keeping all other settings at default values. The results are shown in Table 9, where Sequential-U represents choice (ii) and Sequential-I represents choice (iii). It clearly indicates that Sequential-U is preferable to all the other partitioning methods.

Similarity metric: We experimented with several metrics for measuring similarity between two vectors, including cosine similarity, dot product, and Minkowski distance with different p values. When using Minkowski distance to measure similarity between vectors, we negated the distance to account for the fact that a longer distance indicates a lower similarity. The results of these experiments, shown in Table 10, indicate that cosine similarity is the best choice.

Table 9. Ablation experiment results for choosing the **partitioning method**.

Method	Acc@top1	GFLOPS
Random	79.055%	3.08
Alternate	79.179%	3.08
Sequential-U	79.351%	3.08
Sequential-I	78.898%	3.08
No partition	78.422%	3.08

Table 10. Ablation experiment results for choosing the **similarity metric**.

Similarity	Acc@top1	GFLOPS
dot product	79.257%	3.08
cosine	79.351%	3.08
Manhattan ($p = 1$)	79.208%	3.07
Euclidean ($p = 2$)	79.224%	3.07
Minkowski ($p = 3$)	79.246%	3.07
Minkowski ($p = 4$)	79.273%	3.07
Minkowski ($p = 5$)	79.189%	3.07
Minkowski ($p = \infty$)	79.092%	3.07

G.4. Performance of Zero-TPrune-uni

The ablation experimental results of Zero-TPrune-uni are shown in Table 11. The backbone for deployment is DeiT-S, and the model is evaluated on the ImageNet validation set.

G.5. Hyperparameter Search

The performance of Zero-TPrune, in terms of accuracy, is not sensitive to the hyperparameter setting as long as the number of pruning layers is more than two and the variance of their pruning rate is limited (i.e., the pruning process is not concentrated on one or two layers). We randomly choose different hyperparameter settings and show their performance in Fig. 18. This figure indicates that randomly selecting a hyperparameter setting does not hurt our performance much.

For a fair comparison with baselines, we do not use the best performance we can find through hyperparameter

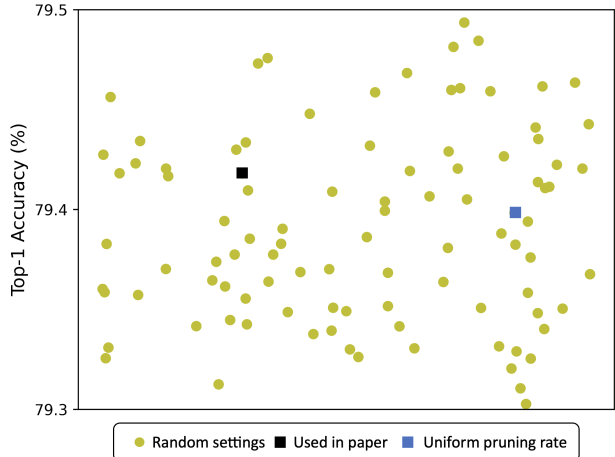


Figure 18. One hundred randomly selected hyperparameter settings and their corresponding performance after being applied to DeiT-S without fine-tuning

search. Instead, we use a hyperparameter setting with approximately the average performance among the search results. It is also close to setting a constant pruning rate across different layers.

Even the full hyperparameter search process is much faster than fine-tuning. For hyperparameter search, we only need to perform inference. Specifically, for MCS, we randomly selected 1024 images in the validation dataset for each hyperparameter setting and obtain the corresponding accuracy. We tried 2000 settings on a single A100 GPU, which only required 3.8 hours. On the contrary, fine-tuning DeiT-S on the ImageNet dataset requires 144 A100 GPU hours.

H. Comparison with State-of-the-Art Methods

In this section, we first supplement comparisons with more depth-adaptive methods in Section H.1 and then compare Zero-TPrune with more straightforward attention-based token ranking methods in Section H.2. Finally, we provide performance comparisons with state-of-the-art fine-tuning-free token pruning methods in terms of throughput in Section H.3.

H.1. Depth-Adaptive Methods

Token pruning can be seen as a fine-grained variant of the depth-adaptive transformer, such as layer dropping. One of our baselines, A-ViT [43], is a token-wise depth-adaptive method. Instead of inserting pruning layers and setting pruning rates for them, it calculates the halting probability per token at each layer and halts tokens at adaptive depth. Zero-TPrune w/o fine-tuning competes with and even outperforms A-ViT w/ fine-tuning, as shown in Fig. 6. A-ViT

Table 11. Contribution breakdown of the different techniques employed in Zero-TPrune-uni. The “-uni” suffix represents uniform initialization in the I-stage.

Acc@1	Params	GFLOPS	Throughput (img/s)	Method
79.8% (base)	22M	4.55G	1505.9	Unpruned model
76.8% (-3.0%)	22M	3.08G	2164.4	random drop
78.0% (+1.2%)	22M	3.08G	2142.3	WPR
78.2% (+0.2%)	22M	3.08G	2139.6	WPR + EIR
78.4% (+0.2%)	22M	3.08G	2107.2	WPR + EIR + VHF (I-stage)
78.9% (+0.5%)	22M	3.08G	2066.4	I-stage + S-stage
79.1% (+0.2%)	22M	3.08G	2062.9	I-stage + S-stage + MC Simulation

Table 12. Comparison with depth-adaptive methods on the DeiT-T model. The performance of Zero-TPrune is obtained without fine-tuning, while other results are obtained with fine-tuning.

Method	Acc@top1	GFLOPS
DeiT-T [36]	71.3%	1.3
ACT [16]	71.0%	1.0
Confidence threshold [23]	65.8%	1.1
Similarity gauging [13]	69.4%	1.1
PonderNet [1]	66.2%	1.0
DynamicViT [30]	70.9%	0.9
A-ViT [43]	71.0%	0.8
Zero-TPrune w/o FT	70.4%	0.9

outperforms prior art on depth-adaptive methods. We adopt corresponding results and compare them with Zero-TPrune in Table 12. Note that the result of Zero-TPrune is obtained off the shelf without fine-tuning, while other results are obtained after fine-tuning the adaptive models.

H.2. Attention-based Token Ranking Methods

One of our baselines, ATS [14], is an attention-based importance ranking method. It uses the attention given by the CLS token to determine the importance of tokens. Simply averaging attention scores in the attention matrix is the baseline of ATS (Fig. 3 in [14]) and performs worse than ATS. For the ablation study, we replace our I-stage with top- k importance selection based on (1) CLS token attention, (2) average attention, and (3) accumulated average attention to improve the effectiveness of our method. Results are shown in Table 13. The batch size is 512 and our **S-stage** is enabled in all settings. We adjust pruning rates slightly to match the FLOPs cost of different settings. Our proposed **I-stage** uses information from all tokens while reducing noise from unimportant tokens, leading to better performance.

Table 13. Performance of pruned DeiT-S models without fine-tuning. Throughput is measured on a single NVIDIA A100 GPU.

Method	Acc@top1	GFLOPS	Throughput(img/s)
DeiT-S	79.8%	4.55	1505.9
CLS Attn.	78.9%	3.00	2179.3
Ave. Attn.	78.4%	2.99	2185.2
Accu. Ave. Attn.	78.5%	2.97	2189.2
I-stage	79.4%	2.97	2188.4

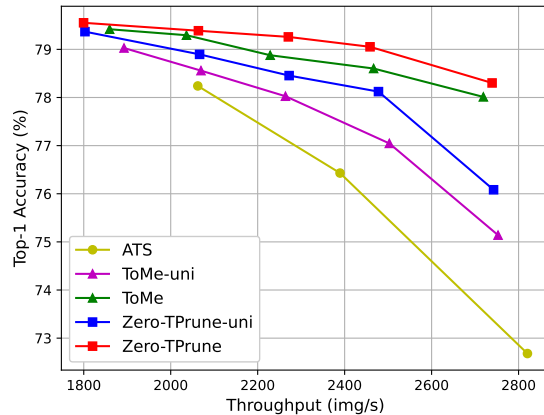


Figure 19. Performance comparison between Zero-TPrune and state-of-the-art fine-tuning-free methods. The applied Transformer backbone is DeiT-S.

H.3. Fine-Tuning-Free Token Pruning Methods

We conduct experiments on DeiT-S to show the superiority of Zero-TPrune over state-of-the-art fine-tuning-free token pruning/merging methods. The experimental results showing the trade-off between accuracy and throughput are shown in Fig. 19.

I. Comparison between Scaling and Pruning

As shown in Table 14, Zero-TPrune cannot outperform all baseline methods when a relatively high pruning rate (e.g.,

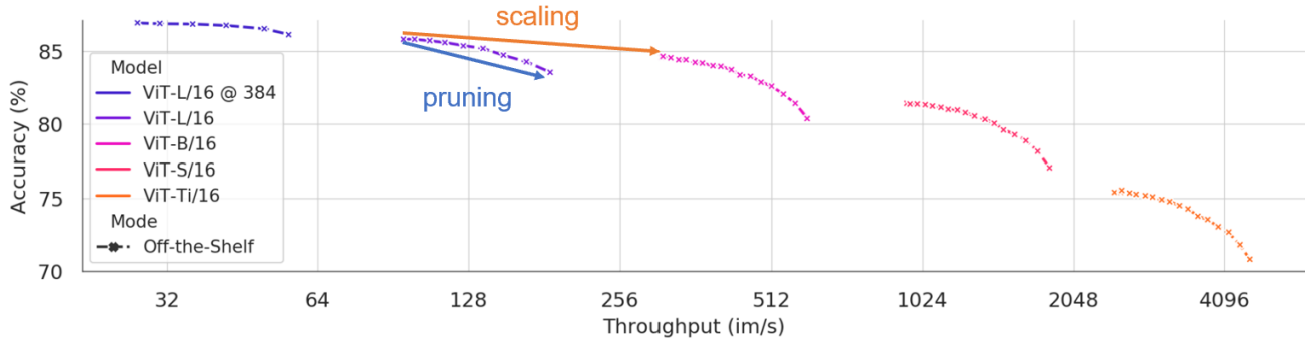


Figure 20. Off-the-shelf performance of ViT models under ToMe [3]. This figure is adopted from [3].

Table 14. Performance of pruned AugReg, LV-ViT, and SWAG models without fine-tuning. SWAG models perform inference on 384px images.

Method	Acc@top1	GFLOPS
LV-ViT-M	84.0%	12.7
+ ATS	80.9%	6.4
+ ToMe	81.6%	6.3
+ Zero-TP	81.4%	6.3
MAE	83.62%	55.4
+ATS	78.39%	29.1
+ToMe	78.95%	28.8
+Zero-TP	78.94%	28.6
SWAG	85.30%	55.6
+ATS	81.03%	27.8
+ToMe	84.59%	28.4
+Zero-TP	84.04%	28.3

although scaling outperforms aggressive pruning in terms of throughput, it achieves lower accuracy than aggressive pruning.

reduce GFLOPS by 50%) is applied to large models (e.g., DeiT-L). However, in this case, scaling to a smaller model is often a better choice. ToMe outperforms Zero-TP when large models are aggressively pruned. Thus, we use the results from ToMe to illustrate this point.

In Fig. 20, ToMe is applied to different ViT backbones with different configurations. Different points on the same curve represent different configurations applied to the same backbone. The first point from the left on each curve represents the unpruned model. Aggressively pruning a model implies switching from the first point from the left on a given curve to the last point on this curve, which increases throughput but suffers from lower accuracy. Switching from the first point from the left on a given curve to the first point on another curve directly scales the size of the model without pruning. Aggressively pruning large models (ViT-L and ViT-B) underperforms scaling them in terms of both accuracy and throughput. On the contrary, for the ViT-S model,